Impacts of Land cover changes on rainfall-runoff and sediment transport processes in the Kelani River

Sudeshika D.M.P.[1*], Imamura Y.[2], Harada D.[3] and Egashira S.[4]

[1]Ph.D. student, Department of Civil & Environmental Engineering, Tokyo Metropolitan University, Japan

[2]Professor, Department of Civil & Environmental Engineering, Tokyo Metropolitan University, Japan

[3]Research Specialist, International Centre for Water Hazards and Risk Management (ICHARM), Public Water Research Institute (PWRI), Japan

[4]Professor, International Centre for Water Hazards and Risk Management (ICHARM), Public Water Research Institute (PWRI), Japan

*pavithrasudeshi@gmail.com (*Corresponding author's email only)

Abstract *The rainfall-runoff and sediment transport processes are significantly influenced by land cover changes. It is crucial to evaluate the effects of land cover changes on these processes for effective river basin management. The Kelani River, a major river in Sri Lanka, is subject to flooding frequently due to urbanization, and its channel bed lowering takes place by approximately 10 cm per year due to excessive sand mining. In this study, we utilized yearly MODIS global land cover data from 2001 to 2022 to evaluate the effects of land cover changes on rainfall-runoff and sediment processes at the basin scale. The RSR model, which is a physically based distributed model that is coupled with the RRI model and Sediment transport process model, was used to simulate these processes. The model was calibrated and validated for the 2016 and 2018 floods. We analyzed the impacts of land cover changes in 2001, 2010, and 2022 on flow discharge, sediment transport rates, and total sediment load in both the lower and upper basin. According to the MODIS land use cover data, among the major land use types in the basin, such as Woody savannas, Forest, Cropland, and Built-up, and the forest area reduced by 15% and 8.3% of the total basin in 2010 and 2022, respectively, compared to 2001. In contrast, the built-up area increased by 0.7% and 2% of the total area in 2010 and 2022, respectively. These changes in land use corresponded to changes in peak flow discharge at the outlet, Hanwella, and Glencourse, which ranged from 1% to -1% for the 10-year flood. For such a small change in runoff, the peak bedload and suspended load rates varied between -1.72 to 7.04 and -4.7 to 25.38, respectively. The research indicated that sediment transport processes are more sensitive to land cover change.*

Keywords: *MODIS land cover, RSR model, Sediment transport rate, Rainfall-Runoff*

Introduction

The Kelani River is significant in Sri Lanka, ranking third in terms of water resources and providing hydropower at its upstream location, as well as supplying 90% of Colombo's drinking water, and industrial sand for an extended period, and supporting a substantial biodiversity ecosystem. However, anthropogenic activities, primarily urbanization and sand mining in the basin, have resulted in riverbed lowering, riverbank erosion, salt intrusion up to

the Ambatale water treatment plant, deterioration of water quality and biodiversity, and flooding in the downstream area (CRIP, 2018).

The alteration and mismanagement of land for various purposes have led to changes in the rainfall-runoff characteristics of the basin, which impact the hydrological and sediment regimes of the basin. It is crucial to consider the effects of land-use changes on hydrological and sediment processes, which can provide valuable information for the development of water resource management and land-use planning strategies (Zuo et al., 2016).

Numerous studies have been conducted to investigate the impacts of land use changes on rainfall-runoff (Choto & Fetene, 2019; Daramola et al., 2022; dos Santos et al., 2020), sediment yield, and soil erosion (Moisa et al., 2021; Sourn et al., 2022). However, these studies have mainly employed simple statistical models or lack physical processes of watersheds. The Rainfall-Sediment-Runoff (RSR) model is a distributed, physically based model, allowing it to consider the temporal and spatial sediment grain size distribution to determine sediment transport rates. In contrast, most sediment models consider a single median grain-size class of sediment, even though bed-material sediment grain size information is critical for understanding riverine sediment processes (Abeshu et al., 2022).

Our study utilized the RSR model to simulate sediment transport processes in the Kelani River basin, considering land use changes from 2001 to 2022. We utilized the MODIS Land Cover Type product (MCD12Q1) with a spatial resolution of 500 m for this purpose. MCD12Q1 is a widely used global land use data product in remote sensing, and it is updated annually, making it highly significant for Earth surface research. One of the main features of this data is spatial and temporal class harmonization, making it an ideal input for hydrological modeling across various regions of the world (Chirachawala et al., 2020).

Methodology

a. Rainfall-Sediment-Runoff Model:

The RSR model is an integration of a rainfall-runoff-inundation (RRI) model and a sediment runoff model that provides flow discharge, bedload, and suspended load rates as outputs. The rainfall-runoff model deals with slopes and river channels, separately and calculates river flow using a 1D diffusion wave equation and flow on slope grids using a 2D diffusion wave equation. The sediment model considers the river network as a series of unit channels, each defined as a channel section with two inflow points and one outflow point. This model does not account for the sediment from the upstream ends of most upstream unit channels due to

the rare occurrence of sediment supply as a form of bedload in the upstream slopes. The governing equations for the RSR model in unit channels are given by the following. The inflow points of the unit channel are represented by x_i and y_i, while the outflow point is represented by x_{i+1}. The continuity equation for flow discharge is

$$\frac{\partial h_{i+1}}{\partial t} = \frac{1}{BL}[Q(x_i) + Q(y_i) - Q(x_{i+1}) + q_{i+1}L_{i+1}] \quad (1)$$

where, h_{i+1}, B, and L are the surface water depth, flow width, and length of the unit channel, t is time, $Q = (1/n)i^{1/2}h^{5/3}B$ where Q, n, i, h, and B are flow discharge, Manning's roughness, bed slope, surface water depth, and flow width, respectively. $Q(x_i)$, $Q(y_i)$ and $Q(x_{i+1})$ are the discharges of the unit channel at inflow points x_i and y_i and outflow point x_{i+1}, respectively.

The convection equation for sediments in suspension is

$$\frac{\partial hC_j}{\partial t} = \frac{1}{(BL)}\{c_{sj}(x_i)Q(x_i) + c_{sj}(y_i)Q(y_i) - c_{sj}(x_{i+1})Q(x_{i+1})\} - D_{sj}(x_{i+1}) + E_{sj}(x_{i+1}) \quad (2)$$

where, $c_j, c_{sj}(x_i)$, $c_{sj}(y_i)$ and $c_{sj}(x_{i+1})$ are the suspended sediment concentration, sediment concentration of the unit channel for sediment size class j at inflow points x_i and y_i and outflow point x_{i+1}, respectively. $D_{sj}(x_{i+1})$ and $E_{sj}(x_{i+1})$ are the deposition and erosion rates of the suspended sediment for the sediment size class j. The deposition and erosion rates are given by Harada et al.'s formulae (2019). $E_{sj} = W_e f_{bj} c_s$ and $D_{sj} = w_{oj} c_j$, where W_e, f_{bj}, c_s, w_{oj}, and c_j are the entrainment velocity, sediment fraction, sediment concentration of the bedload layer, settling velocity, and suspended sediment concentration for sediment size class j, respectively.

The sediment continuity equation is

$$\frac{\partial z}{\partial t} = \frac{1}{(1-\lambda)}\sum_j[\frac{1}{BL}\{Q_{bj}(x_i) + Q_{bj}(y_i) - Q_{bj}(x_{i+1})\} + D_{sj}(x_{i+1}) - E_{sj}(x_{i+1})] \quad (3)$$

where z is the riverbed elevation, λ is the porosity of bed sediment, $Q_{bj}(x_i)$, $Q_{bj}(y_i)$, and $Q_{bj}(x_{i+1})$ are the bedload rates of the unit channel for the sediment size class j at inflow points x_i and y_i and outflow point x_{i+1}, respectively. Bedload rates are given by Egashira et al.'s formulae (1997, 2005) as $q_{b*j} = 4.4\, p_j \tau_{*j}^{5/2}$ which is similar to $q_{bj}/\sqrt{(s-1)gd^3}$, where q_{b*}, s, d, and τ_{*j} are the non-dimensional bedload rate per unit time and unit length, the relative density of the sediment particles, sediment size, and non-dimensional bed shear stress respectively. The factor of 4.4 is an estimated parameter following the original formulae.

The temporal change of sediment grain size fraction for the first layer of each unit channel is

$$\frac{\partial P_j}{\partial t} = \frac{1}{(1-\lambda)\delta BL}\{Q_{bj}(x_i) + Q_{bj}(y_i) - Q_{bj}(x_{i+1})\} + D_{sj}(x_{i+1}) - E_{sj}(x_{i+1}) - \frac{\partial z}{\partial t}\frac{f_j}{\delta} \quad (4)$$

where $\sum_1^N p_j = 1$, $f_j = \begin{cases} p_{j2} \; when \; \frac{\partial z}{\partial t} \leq 0; \; p_j \; when \; \frac{\partial z}{\partial t} > 0 \end{cases}$

p_j is the fraction of sediment size class j, δ is the depth of the surface layer, p_{j2} is the fraction of sediment size class j in the second layer underneath the exchange layer.

b. Study area:

The Kelani River Basin (Figure 1) is located between latitudes of 6° 47' and 7° 05' and longitudes of 79° 52' and 80° 13', spanning an area of 2,230 km^2 in the wet zone of Sri Lanka shown in Figure 1. The Kelani River is significant in Sri Lanka and flows towards the west coast of the country through Colombo, the Capital of the country. It supplies 80% of Colombo's drinking water needs and is used for hydropower generation in the upstream region. The basin experiences a mean annual rainfall of 3,718 mm, primarily due to the southwest monsoon. The terrain of the basin naturally divides it into two basins: the upper basin, which is characterized by steep terrain, and the lower basin, which is a floodplain (De Silva et al., 2012). The lower basin is prone to frequent flooding due to its orientation, topography, and poor drainage (Dissanayaka & Rajapakse, 2019).

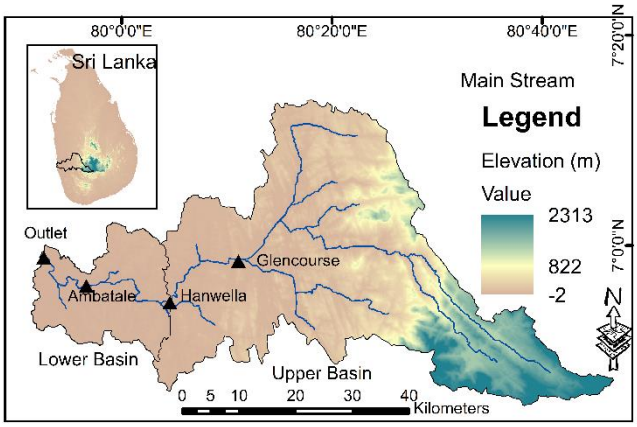

Figure 1: Study map

c. MODIS yearly Global Land use data:

The Moderate Resolution Imaging Spectrometer (MODIS) yearly global land cover product (MCD12Q1) with a spatial resolution of 500 m for 2001, 2010, 2016, 2018, and 2022 was downloaded from the USGS Earth Explorer website. The land-use maps were reclassified according to the International Geosphere-Biosphere Program (IGBP) global vegetation classification scheme (Sulla-Menashe & Friedl, 2018) in Table 1 for the years 2001, 2010, 2016, 2018, and 2022. In addition, these maps were verified based on the maps revised by the Survey Department, Sri Lanka.

Table 1: IGBP classification for the major land use types in the Kelani River Basin

Land use type	Definition
Evergreen broad-leaf Forests	Dominated by evergreen broadleaf and palmate trees with canopy height exceeding 2 m and tree cover exceeding 60%.
Woody Savannas	Lands with canopy height exceeding 2 m and tree cover between 30 and 60%.
Croplands	At least 60% of the land is covered by cultivated cropland.
Urban	At least 30% of the land is impervious surface area.

d. Topographic data:

Hydrological data and maps based on SHuttle Elevation Derivatives at multiple Scales (HydroSHEDS) 15-arc (~500 m) digital elevation model (DEM) were used for delineating topographic maps such as elevation, flow accumulation, and flow direction for the basin using the ArcGIS hydro tools.

e. Soil map data:

FAO/ UNESCO soil map of the world at 1: 5 000 000 scale was used to classify the soil texture classification over the basin to define the soil properties shown in Figure 2. Soil properties according to soil texture classification are given in Table 2.

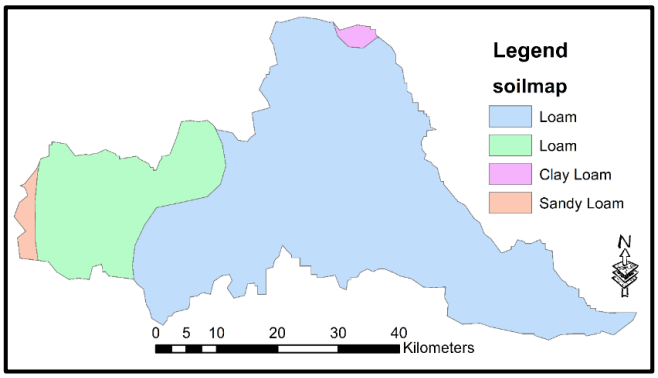

Figure 2: Soil map of the Kelani River Basin

Table 2: Porosity for each soil texture

Soil Texture	Loam	Clay Loam	Sandy Loam
Porosity	0.463	0.464	0.453

e. RSR model simulation conditions:

RSR model calibration and validation were carried out for the flood events in 2016 and 2018, respectively, for both the Rainfall-runoff model and sediment model using the observed hourly discharge data at Glencourse and measured hourly sediment concentration at the Ambatale water treatment plant. Here, sediment concentration data

were determined based on the turbidity measurements at the Ambatale water treatment plant using the portable turbidity meter HACH 2100 P. The results of calibration and validation of the rainfall-runoff model are given in Figure 3. The rainfall-runoff model performed well for the 2016 and 2018 floods with the Nash-Sutcliff coefficient of 0.8 and 0.7, respectively.

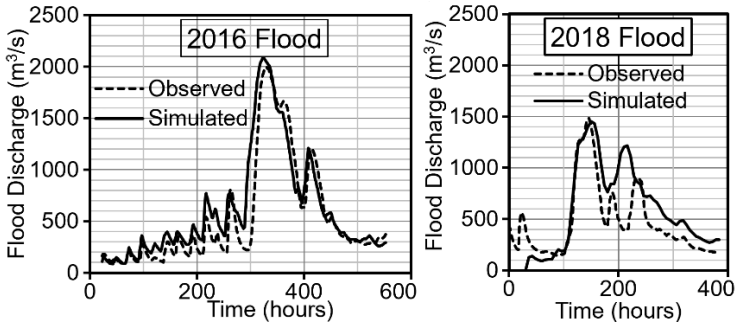

Figure 3: Rainfall-runoff model calibration and validation

Accordingly, the calibrated parameter values are 0.04, 1 m, and 0.085 for Manning's roughness of the river channel, soil depth, and lateral saturated hydraulic conductivity respectively. Here, we defined the effective Manning's roughness of slopes (n_s) based on the land use type, and soil porosity (p) based on soil texture through the literature (Pakoksung, 2016) as given in Table 3.

Table 3: Manning's roughness and soil porosity of each land use type

Land use	Forest	Woody savannas	Grassland	Wetland	Cropland	Urban	Water bodies
n_s	0.85	0.45	0.3	0.5	0.3	0.05	0.05
p	0.463	0.463	0.463	0.463	0.463	0.001	0.463

The results of calibration and validation of the sediment model are given in Figure 4.

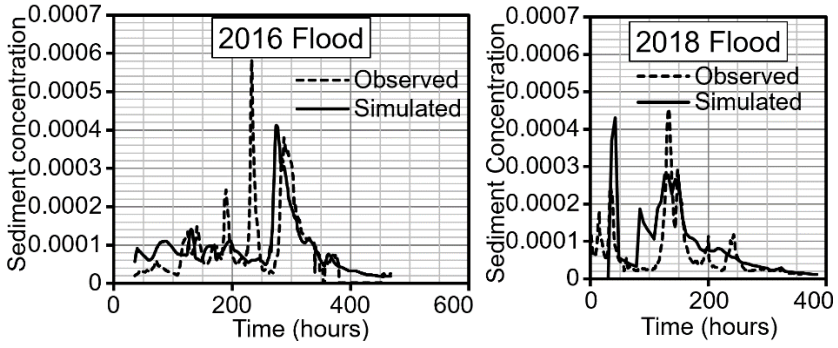

Figure 4: Sediment model calibration and validation

The initial sediment grain size distribution in Table 4 was defined by calibrating the model and considering field data measured during January 2023.

Table 4: Initial sediment grain size distribution

Sediment grain size mm	0.037	0.11	0.225	0.45	0.89	1.77	3.55	8.72	31.35	700	1200
Fraction %	0	0	1	3	7	10	19	28	28	2	2

To investigate the land use impacts on rainfall-runoff and sediment transport processes for 2001, 2010, and 2022, the simulations of the RSR model were carried out using the 2016 flood (10-year flood) data using corresponding land use maps of the year for 2001, 2010, and 2022. The parameters were defined according to the land use types given in Table 3.

g. Sediment erodibility/ landslide index:

The Shuttle Radar Topography Mission (SRTM) 3-arc (90 m) DEM was utilized to determine sediment erodibility and the landslide index. The sediment erodibility of a surface area is dependent on the bed shear stress, which can be represented as $\tau = hi\rho g$, where h is the surface water depth, i is the bed slope, ρ is the water density, and g is the gravitational acceleration. In this context, ρ and g remain constant. Thus, sediment erodibility can be expressed as:

$$Sediment\ erodibility = hi \quad (5)$$

The landslide index is influenced by subsurface flow, and thus, it can be defined as:

$$Landslide\ Index = h_s i/d \quad (5)$$

where h_s is the subsurface water depth, and d is the soil depth. Here, h and h_s are determined using the RRI model that was developed using the Shuttle Radar Topography Mission (SRTM) 3-arc (90 m) DEM.

The calibration results of the RRI model are presented in Figure 5, and the calibrated parameters are 0.04, 0.85, 2m, 0.025, and 1500 for effective Manning's roughness for river channel, effective Manning's roughness for slope cells, soil depth, saturated hydraulic conductivity, and threshold, respectively.

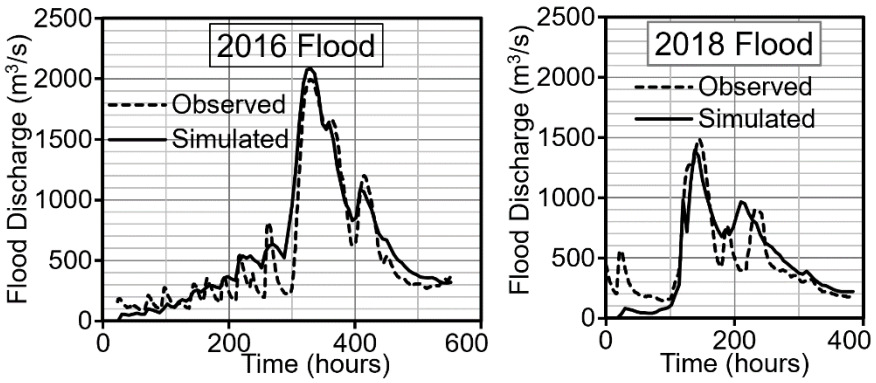

Figure 5: RRI model's calibration and validation results

Figure 6 depicts the values of h, h_s, and i over the basin for the 2016 flood (10-year flood).

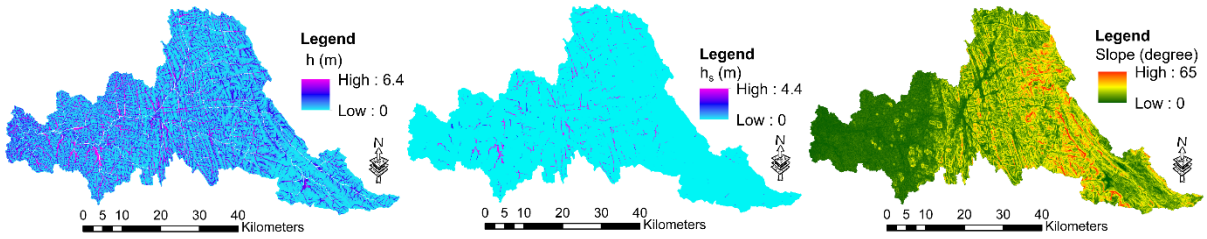

Figure 6: h, h_s, and i for a 10-year flood

Results and Discussion

a. Land-use change analysis:

Figure 7 shows the MODIS land cover map for the years 2001, 2010, and 2022 prepared according to the IGBP classifications in Table 1. According to Figure 7, the Kelani River Basin comprises four major land use types, namely Forest, Cropland, Woody Savannas, and Urban areas. The upper basin is predominantly covered by woody savannas and forest areas, while downstream areas are dominated by cropland and urban areas.

Accordingly, the area percentage of the major land use types in the Kelani River basin for 2001, 2010, and 2022 are illustrated in Figure 8. In all years, 2001, 2010, and 2022, woody savannas account for the majority of the area, exceeding 48%. Forest areas were 33% in 2001 but depleted to around 20% by 2010 and 2022. Cropland and urban areas constituted approximately 13% and 7% of the area, respectively.

Figure 9 displays the changes in the area percentage of the major land use types in 2010 and 2022, compared to the year 2001. Urban areas and woody savannas show an increasing trend, while cropland and forest areas exhibit a decreasing trend. In 2010, forest areas decreased by approximately 15%, while woody savannas increased by the same amount. By 2022, the forest area had increased by approximately 5% compared to 2010, while woody savannas had

reduced by 7% compared to 2010. Urban areas increased by only 0.7% and 2% in 2010 and 2022, respectively, compared to 2001.

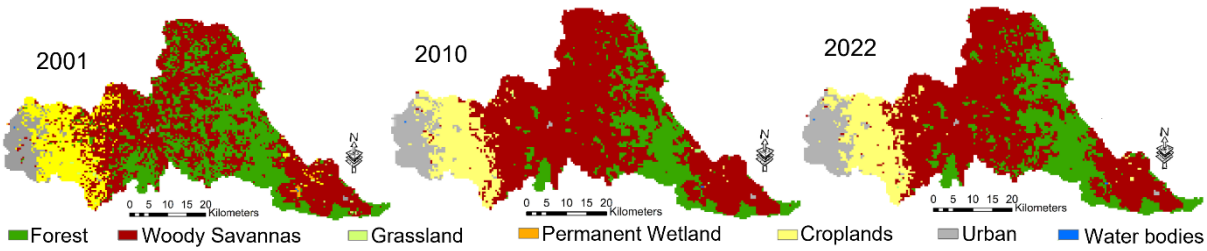

Figure 7: MODIS land cover maps for 2001, 2010, and 2022

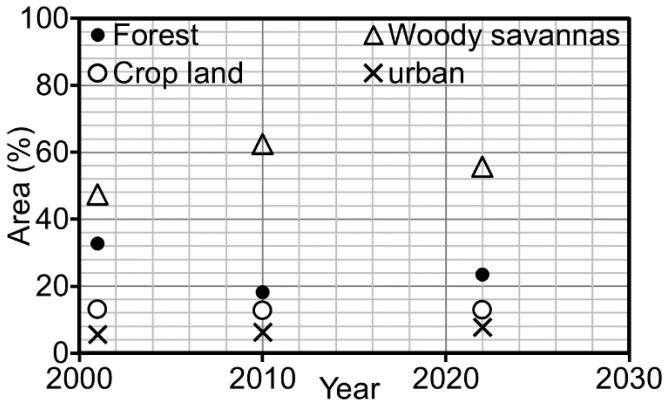

Figure 8: Total land use area (%) for 2001, 2010, and 2022

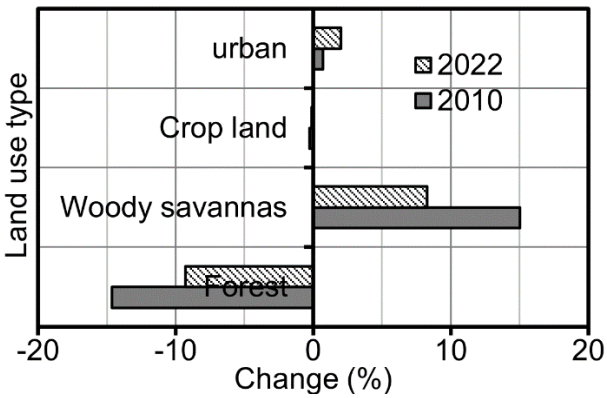

Figure 9: Land use change in (%) in 2010 and 2022 compared to 2001

b. Runoff variation for 10-year flood:

Figure 10 illustrates the variations in runoff for the 2016 flood (10-year flood) at outlet, Hanwella, and Glencourse in Figure 1 for the years 2001, 2010, and 2022. The data presented in Figure 10 shows that the runoff variation at outlet, Hanwella, and Glencourse for the years 2001, 2010, and 2022 is almost identical. Table 5 provides peak discharge values at each location for 2001, 2010, and 2022. As can be observed from Table 5, the peak discharge at all selected locations in 2010 is slightly higher than in 2001 and 2022 due to the depletion of the

forest area in 2010 compared to the years 2001 and 2022. The peak discharge at Hanwella and Glencourse in 2010 and 2022 is slightly higher than in 2001 due to the depletion of the forest area compared to the year 2001, where both locations' upstream land area is covered predominantly by forest and woody savannas. The peak discharge changing percentage at Outlet, Hanwella, and Glencourse in 2010 compared to 2001 are about 0.4%, 1%, and 1%, respectively, while the peak discharge changing percentage at Outlet, Hanwella, and Glencourse in 2022 compared to 2001 are about -0.14%, 0.1%, and 0.34%, respectively.

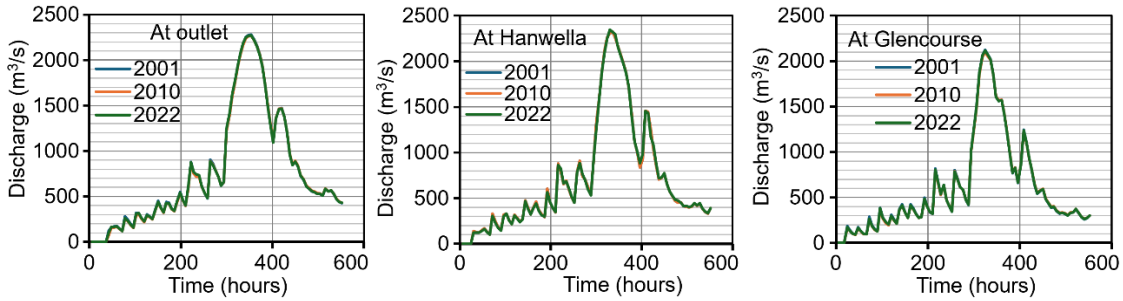

Figure 10: Flow runoff variation at each location for 2001, 2010, and 2022

Table 5: Peak flow discharge at each location for 2001, 2010, and 2022

Location	Outlet	Hanwella	Glencourse
2001	2,255	2,283	2,048
2010	2,264	2,306	2,069
2022	2,251	2,285	2,055

c. Bedload rate and Suspended load rate variation for the 10-year flood:

Figure 11 and 12 depict the variations in bedload and suspended load rates, respectively, at Outlet, Hanwella, and Glencourse. The data presented in Figure 11 and 12 indicates that the variation of bedload and suspended load rates in 2010 is slightly higher at peaks compared to the years 2001 and 2022 due to the low forest area in 2010 compared to the years 2001 and 2022, which caused the high peak discharge in 2010 presented in Table 5. Table 6 provides the peak bedload and suspended load rates at Outlet, Hanwella, and Glencourse for 2001, 2010, and 2022. As can be observed from Table 6, the peak bedload and suspended load rates in 2010 are higher than in 2001 and 2022 due to the peak discharge. The bedload and suspended load rates at Outlet and Hanwella in 2022 were slightly lower than in 2001 and 2010, possibly due to variations in flow, sediment grain size, and riverbed elevations caused by land use changes. However, at Glencourse, the peak bedload and suspended load rates in 2010 and 2022 were higher than in 2001, likely due to the depletion of the forest area. The percentage changes in peak bedload rates in 2010 were 2.4%, 3.4%, and 7.04% at Hanwella,

Glencourse, and Outlet, respectively, while the changes in peak suspended load rates were 2.2%, 2.3%, and 25%, at Hanwella, Glencourse, and Outlet, respectively. The variation in peak bedload and suspended load rates at Glencourse was higher than at Outlet and Hanwella due to its greater sensitivity to changes in the upstream forest layer.

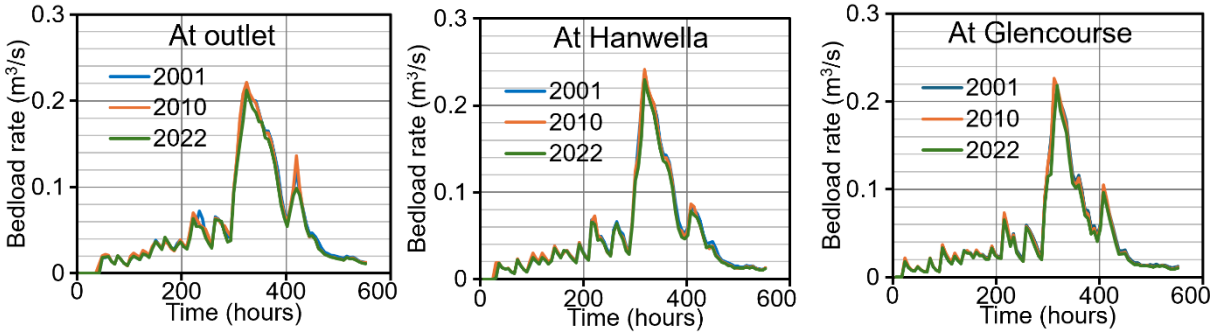

Figure 11: Bedload rate variation at Outlet, Hanwella, Glencourse for 2001, 2010, and 2022

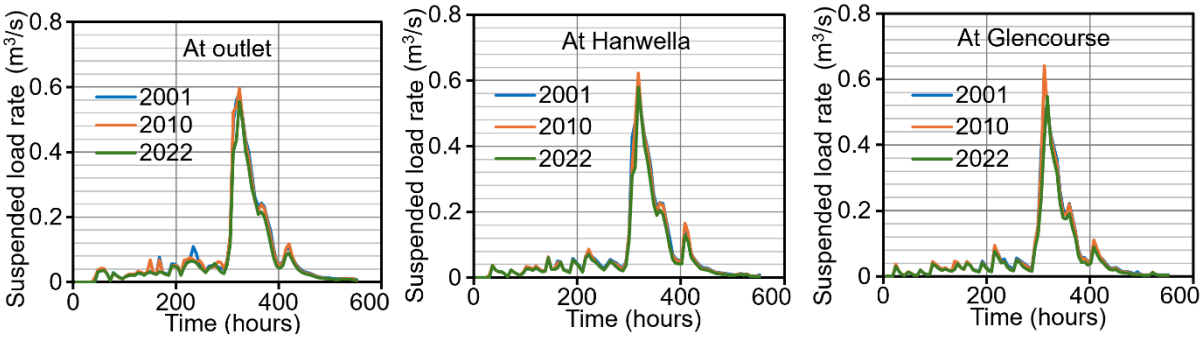

Figure 12: Suspended load rate at each location for 2001, 2010, and 2022

Table 6: Peak discharge at Outlet, Hanwella, and Glencourse for 2001, 2010, and 2022

Year	Bedload rate (m^3/s)			Suspended load rate (m^3/s)		
	Outlet	Hanwella	Glencourse	Outlet	Hanwella	Glencourse
2001	0.2160	0.2338	0.2116	0.5828	0.6087	0.5117
2010	0.2213	0.2415	0.2265	0.5958	0.6225	0.6416
2022	0.2120	0.2298	0.2182	0.5554	0.5799	0.5473

d. Total bedload and Suspended load for the 10-year flood:

Figure 13 displays the total load at the three locations in 2001, 2010, and 2022. The total load is calculated as the total area under both bedload and suspended load rate curves shown in Figures 11 and 12. The total load in 2022 was lower than in 2001 and 2010 at all three locations, with no significant difference between 2001 and 2010. These differences occurred due to variations in flow, riverbed, and sediment grain size. The decrease in suspended load

in 2010 and 2022 was greater than the decrease in bedload, indicating that suspended load is more sensitive than bedload due to sediment transport being dominated by suspension at the selected locations.

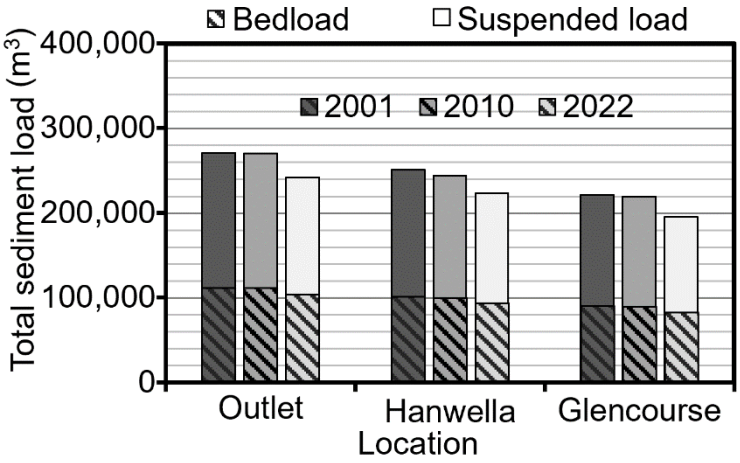

Figure 13: Total sediment load at each location for 2001, 2010, and 2022

e. Mean diameter variation of riverbed material for the 10-year flood:

Figure 14 presents the average diameter fluctuation of riverbed material at the outlet, Hanwella, and Glencourse during the 10-year flood in 2001, 2010, and 2022. As illustrated in Figure 14, there is a slight variation in the mean diameter of bed material in 2001, 2010, and 2022. During the flood event, the riverbed material becomes coarser due to increased sediment transport capacity resulting from increased flow discharge. Following the flood, the riverbed material suddenly becomes finer with reduced discharge, eventually reaching a stable sediment condition in the riverbed.

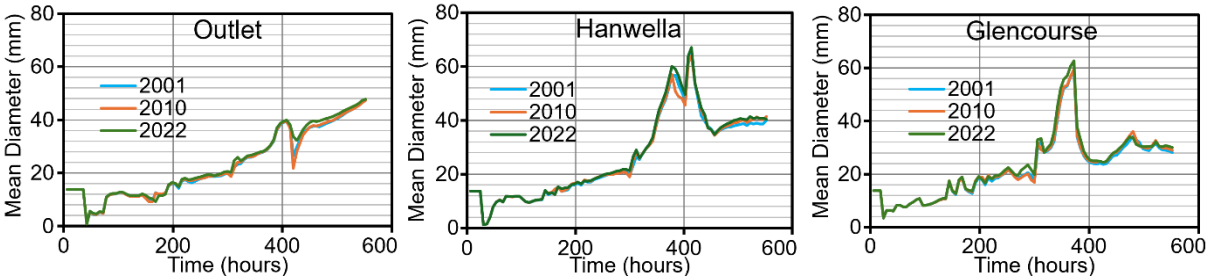

Figure 14: Mean diameter variation at each location for 2001, 2010, and 2022

f. Riverbed variation for 10-year flood:

Figure 15 displays the overall riverbed elevation change in 2001, showing the difference in total riverbed elevation in 2010 and 2022 compared to 2001 for 2016 flood (10-year flood). As shown in Figure 15, most of the downstream channels experience erosion of 0 to 0.5 m, while there is a trend of deposition in the upstream channels. The tendencies of erosion or

deposition in the channels are influenced by factors such as river morphology, hydraulics, and hydrological conditions. The difference in deposition or erosion elevation of riverbeds in 2010 and 2022 compared to 2001 ranges from 0 cm to 9 cm due to land use changes, indicating that changes in riverbed elevation due to land use changes are substantial. These changes in riverbed elevation led to changes in sediment transport as well as water depths.

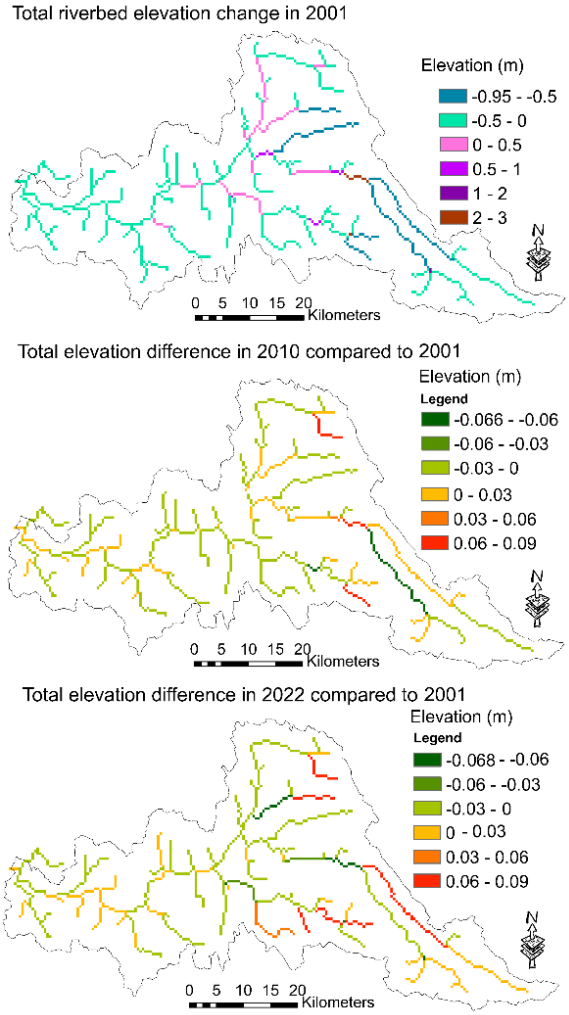

Figure 15: Total riverbed elevation changes in 2001 and the total riverbed elevation difference in 2010, and 2022 compared to 2001

e. Sediment erodibility/ landslide index:

Figure 16 displays the erodibility and landslide index along with historical landslides from 2003 to 2022. The sediment erodibility and landslide index are higher in the middle of the Kelani River Basin, indicating that landslides are more likely to occur in that region. According to the historical landslides from 2003 to 2022, landslides have occurred in areas where sediment erodibility and landslide index are high. Furthermore, the high landslide

index observed in the downstream region can be noted, despite the terrain being flat and the slope size insignificant in Figure 6. Consequently, although the landslide index is elevated, the likelihood of landslide occurrence remains minimal.

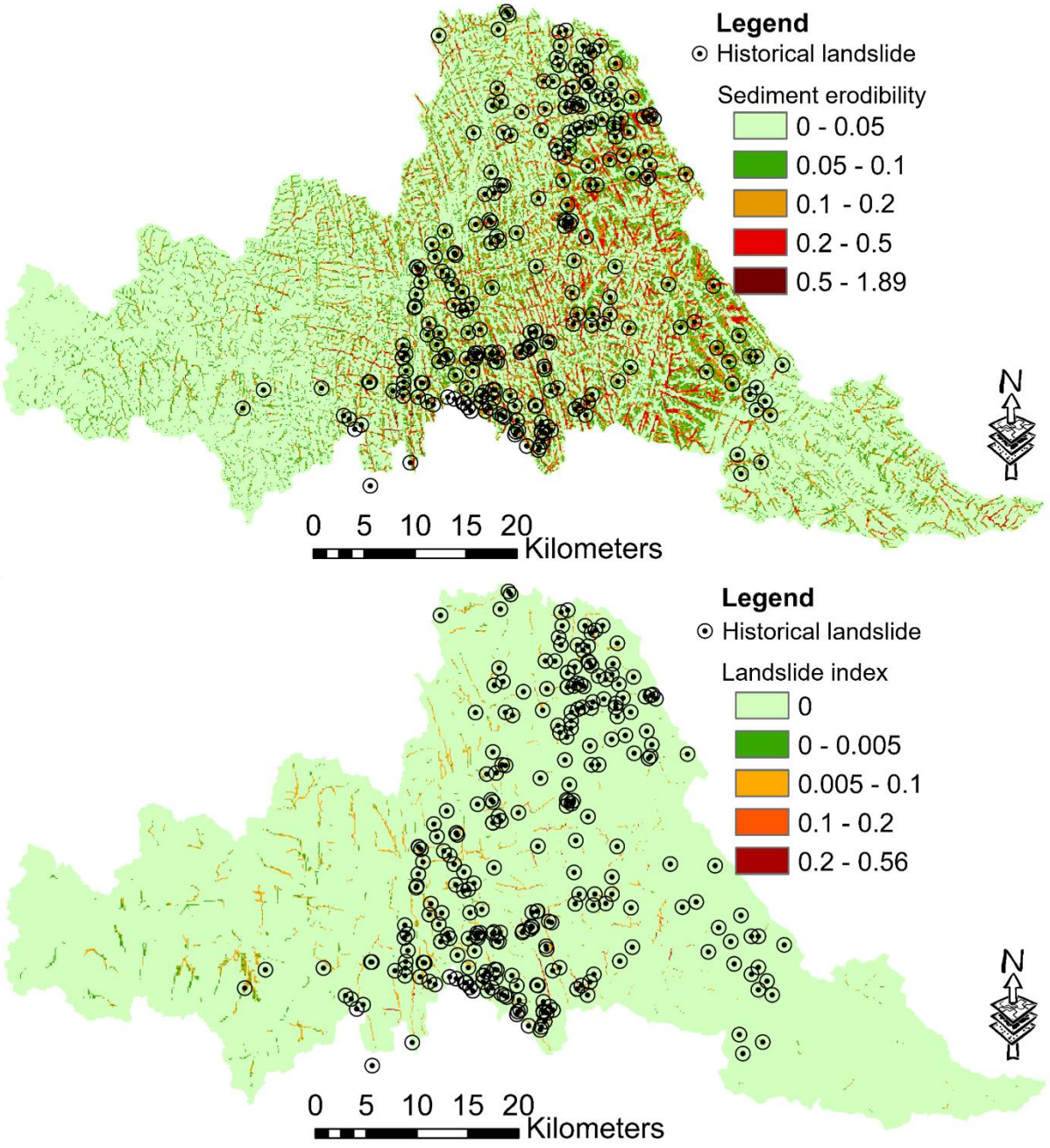

Figure 16: Erodibility and landslide index with historical landslide from 2003 to 2022

Conclusions

The study found that sediment transport processes in the basin are more susceptible to change than rainfall-runoff processes. The total sediment loads for both 2010 and 2022 exhibit a downward trend, with a more pronounced decrease in 2022 compared to 2001. This decrease

can be attributed to changes in land use, resulting in a reduction of approximately 10%. The alteration in riverbed elevation due to land use change is significant, varying between 0 and 9 cm compared to 2001. The middle region of the basin is particularly vulnerable to landslides and soil erodibility, as evidenced by higher erodibility and landslide index values in this area. Moreover, there has been an increasing trend in woody savanna and urban areas, while forest and cropland areas have experienced a decline in both 2010 and 2022 compared to 2001. Among the main land use types in the basin, which include woody savannas, forest, cropland, and urban areas, changes in woody savannas and forest in 2010 and 2022 compared to 2001 are particularly notable.

Acknowledge

The Authors wish to thank the International Centre for Water Hazard and Risk Management (ICHARM) for the RSR model access, the Irrigation Department, the Meteorology Department, the National Water Supply and Drainage Board, the National Building Research Organization of Sri Lanka for the meteorological, hydrological, and landslide data, the National Aeronautics and Space Administration (NASA), United States Geological Survey (USGS), World Wildlife Fund (WWF), and Food and Agriculture Organization of the United Nations (FAO) for open access satellite data, and the Department of Civil Engineering of the University of Moratuwa for the laboratory facilities, and Dr. Toru Konishi, and Prof. Hideo Amaguchi for feedback.

Funding statement

This research was supported by the Tokyo Metropolitan Government Advanced Research Grant Number (R4-2).

References

Abeshu, G. W., Li, H. Y., Zhu, Z., Tan, Z., Leung, L. R., & Li, H. Y. (2022). Median bed-material sediment particle size across rivers in the contiguous US. *Earth System Science Data*, *14*(2), 929–942. https://doi.org/10.5194/ESSD-14-929-2022

Chirachawala, C., Shrestha, S., Babel, M. S., Virdis, S. G. P., & Wichakul, S. (2020). Evaluation of global land use/land cover products for hydrologic simulation in the Upper Yom River Basin, Thailand. *Science of The Total Environment*, *708*, 135148. https://doi.org/10.1016/J.SCITOTENV.2019.135148

Choto, M., & Fetene, A. (2019). Impacts of land use/land cover change on stream flow and sediment yield of Gojeb watershed, Omo-Gibe basin, Ethiopia. *Remote Sensing Applications: Society and Environment*, *14*, 84–99. https://doi.org/10.1016/J.RSASE.2019.01.003

CRIP. (2018). *Climate Resilience Improvement Project; Strategic Environmental Assessment of Development of river basin level flood and drought mitigation Investment plans (DBIP)*.

Daramola, J., Adepehin, E. J., Ekhwan, T. M., Choy, L. K., Mokhtar, J., & Tabiti, T. S. (2022). Impacts of Land-Use Change, Associated Land-Use Area and Runoff on Watershed Sediment Yield: Implications from the Kaduna Watershed. *Water 2022, Vol. 14, Page 325*, *14*(3), 325. https://doi.org/10.3390/W14030325

De Silva, M. M. G. T., Weerakoon, S. B., Herath, S., Ratnayake, U. R., & Mahanama, S. (2012). Flood Inundation Mapping along the Lower Reach of Kelani River Basin under the Impact of Climate Change. *Engineer: Journal of the Institution of Engineers, Sri Lanka*, *45*(2), 23. https://doi.org/10.4038/ENGINEER.V45I2.6938

Dissanayaka, K. D. C. R., & Rajapakse, R. L. H. L. (2019). Long-term precipitation trends and climate extremes in the Kelani River basin, Sri Lanka, and their impact on streamflow variability under climate change. *Paddy and Water Environment*, *17*(2), 281–289. https://doi.org/10.1007/S10333-019-00721-6/TABLES/5

dos Santos, F. M., de Oliveira, R. P., & Di Lollo, J. A. (2020). Effects of Land Use Changes on Streamflow and Sediment Yield in Atibaia River Basin—SP, Brazil. *Water 2020, Vol. 12, Page 1711*, *12*(6), 1711. https://doi.org/10.3390/W12061711

Egashira, S., & Itoh, T. (2006). Paradoxical discussions on sediment transport formulas. *River, Coastal and Estuarine Morphodynamics: RCEM 2005 - Proceedings of the 4th IAHR Symposium on River, Coastal and Estuarine Morphodynamics*, *1*, 33–38. https://jglobal.jst.go.jp/en/detail?JGLOBAL_ID=201902218923712199

Egashira, S., Miyamoto, K., & Ito, T. (1997). Bed-load Rate in View of Two Phase Flow Dynamics. *Proceedings of Hydraulic Engineering*, *41*, 789–794. https://doi.org/10.2208/PROHE.41.789

Harada, D., Egashira, S., Ahmad, T. S., & Katayama, N. (2019). A study on the erosion rate of riverbeds using the entrainment concept. *Journal of Hydraulic Engineering*, *75*(2), I_967-I_972. https://doi.org/10.2208/JSCEJHE.75.2_I_967

Moisa, M. B., Negash, D. A., Merga, B. B., & Gemeda, D. O. (2021). Impact of land-use and land-cover change on soil erosion using the RUSLE model and the geographic information system: a case of Temeji watershed, Western Ethiopia. *Journal of Water and Climate Change*, *12*(7), 3404–3420. https://doi.org/10.2166/WCC.2021.131

Pakoksung, K. (2016). *Runoff Analysis using Satellite Data for Regional Flood Assessment - Spatial and Time Series Bias Correction of Satellite Data -*. 高知工科大学. https://kutarr.kochi-tech.ac.jp/records/600

Sourn, T., Pok, S., Chou, P., Nut, N., Theng, D., & Vara Prasad, P. V. (2022). Assessment of Land Use and Land Cover Changes on Soil Erosion Using Remote Sensing, GIS and RUSLE Model: A Case Study of Battambang Province, Cambodia. *Sustainability 2022, Vol. 14, Page 4066*, *14*(7), 4066. https://doi.org/10.3390/SU14074066

Sulla-Menashe, D., & Friedl, M. A. (2018). *User Guide to Collection 6 MODIS Land Cover (MCD12Q1 and MCD12C1) Product*. https://lpdaac.usgs.gov/products/mcd12q1v006/

Zuo, D., Xu, Z., Yao, W., Jin, S., Xiao, P., & Ran, D. (2016). Assessing the effects of changes in land use and climate on runoff and sediment yields from a watershed in the Loess Plateau of China. *Science of The Total Environment*, *544*, 238–250. https://doi.org/10.1016/J.SCITOTENV.2015.11.060